Interlayer diffusion of Au atoms in a heteroepitaxial system

2009 J. Phys.: Condens. Matter 21 474210

(http://iopscience.iop.org/0953-8984/21/47/474210)

J. Phys.: Condens. Matter **21** (2009) 474210 (8pp) doi:10.1088/0953-8984/21/47/474210

Interlayer diffusion of Au atoms in a heteroepitaxial system

Shohei Ogura and Katsuyuki Fukutani

Institute of Industrial Science, University of Tokyo, 4-6-1 Komaba, Meguro-ku, Tokyo 153-8505, Japan

E-mail: ogura@iis.u-tokyo.ac.jp

Received 2 April 2009
Published 5 November 2009
Online at stacks.iop.org/JPhysCM/21/474210

Abstract

In heteroepitaxy, thin-film growth proceeds in two-dimensional layer-by-layer, three-dimensional island, or layer-plus-island modes depending on the growth conditions. Interlayer mass transport plays a crucial role in determining the growth mode. We investigate interlayer diffusion of Au atoms from Au islands grown on Ir(111) by scanning tunneling microscopy (STM) and kinetic Monte Carlo (KMC) simulations. STM measurements reveal that the first Au layer on Ir(111) grows in a complete layer at 100 K, whereas the Au layer grows in a three-dimensional fashion from the second Au layer at this temperature. Annealing these surfaces to 300 K reduces the higher-layer islands, indicating that Au atoms undergo step-down diffusion. By measuring the density of the top-layer islands and comparing them with the KMC simulation results, the additional step-down diffusion barrier for Au atoms to descend from the Au islands is estimated to be 0.02 eV on the first Au layer and 0.04 eV on the second Au layer. The layer dependence of the additional step-down diffusion barrier is explained in terms of the lattice mismatch between Au and underlying layers.

1. Introduction

Surface diffusion is a fundamental process involved in a variety of phenomena such as thin-film growth and catalytic reactions. In thin-film growth, the growth mode, i.e. whether the film grows in a two-dimensional or three-dimensional fashion, is determined by interlayer mass transport across surface steps. Under a thermodynamic equilibrium condition where the interlayer mass transport is sufficiently fast, the growth mode is determined by the balance of the surface and interface free energies. Thus, the film structure with the smallest free energy is formed. In the kinetic regime where the growth proceeds far from thermal equilibrium, on the other hand, the growth mode is determined by the step-crossing diffusion rate with respect to the rates of other kinetic processes such as deposition and terrace diffusion. It is widely accepted that adatoms feel an additional barrier to cross the step in addition to the diffusion barrier on a flat terrace. As shown in figure 1, when atoms descend from an island, they feel an additional diffusion barrier caused by the lower coordination number at the transition state (A in figure 1). On the other hand, the island edge (B in figure 1) is energetically more favorable due to the higher coordination number. The additional barrier for the step-down diffusion is commonly called the Ehrlich–Schwoebel (ES) barrier [1, 2]. When the ES barrier is smaller, films tend to grow in a layer-by-layer fashion, whereas they tend to grow in a multilayer mode when the ES barrier is higher. To control the growth mode, it is necessary to understand the step-crossing diffusion coefficient. Field ion microscopy (FIM) [3, 4] and scanning tunneling microscopy (STM) [5, 6] are powerful tools to investigate the step-crossing diffusion. The step-down and step-up diffusions of Ir atoms across the step on Ir(111) were investigated by FIM [3, 4]. In STM measurements, the nucleation probability of the top-layer islands is investigated. The data are compared to the critical island radius theory [5], and the step-down diffusion barrier can be estimated. Kinetic Monte Carlo (KMC) simulations can also be used to derive the ES barrier by searching for parameters that reproduce observed structures [7].

Au thin films grown on Ir(111) are reported to have an anomalous chemical reactivity for H_2 dissociative adsorption [8–11]. Although the island structure is expected to affect the reactivity, the origin of the anomalous reactivity still remains an open question. Synthesizing Au nanoparticles with various shapes is desired to tailor surfaces with catalytic activities on one hand [12, 13], on the other hand chemically

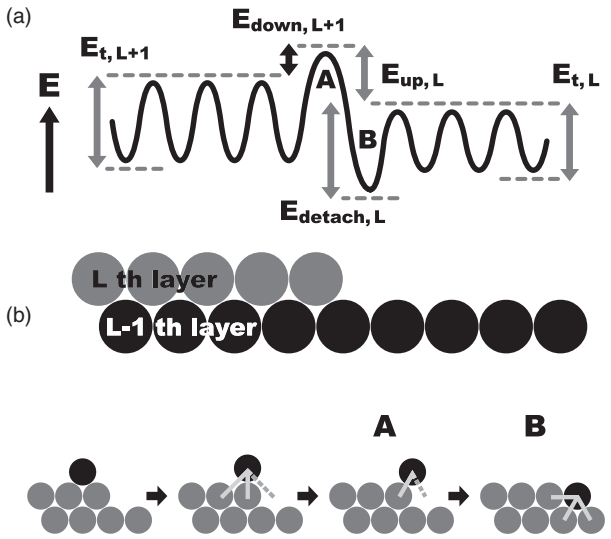

Figure 1. (a) Schematic energy diagram for an adatom at the step (side view). (b) Schematic illustration of the coordination number during the step-down diffusion.

inert flat surfaces are required for atom lenses or mirrors [14]. Thus, knowledge on detailed mechanisms of interlayer diffusion and quantitative determination of its rate are highly desirable.

In the present study, we investigate the interlayer diffusion of Au atoms on Au islands grown on Ir(111) by measuring the Au growth on Ir(111) with STM. The first Au layer is found to grow in a complete layer at 100 K, whereas higher Au layers are found to grow in a three-dimensional mode. Furthermore, the number of the higher-layer islands decreases by annealing the surfaces to 300 K. Histograms of the exposed coverage show occurrence of step-down diffusion. By performing KMC simulations, we estimate the ES barrier to be 0.02 eV on the first Au layer and 0.04 eV on the second Au layer. The layer dependence of the ES barrier is explained by the enhanced exchange diffusion due to the lattice mismatch between Au and underlying layers.

2. Experimental procedure

The experiments were performed in an ultrahigh vacuum chamber equipped with a four-grid optics for low-energy electron diffraction (LEED) and Auger electron spectroscopy (AES), and a variable-temperature STM system (Omicron VT-AFM/STM). The base pressure of the chamber was typically 1×10^{-9} Pa. An Ir crystal (Surface Preparation Laboratory) with a thickness of 1 mm oriented in the (111) direction with an accuracy of $\pm 0.1°$ was cut to a size of 3×3 mm^2 and attached to the Omicron sample holder for direct heating. The Ir(111) sample was cleaned by cycles of 0.5 keV Ar^+ sputtering, annealing in 8×10^{-6} Pa O_2 atmosphere at 1100 K, and final flashing to 1500 K [8]. The surface cleanliness was checked by LEED, AES, and STM. Au deposition was conducted using heated tungsten filaments loaded with an Au wire at a rate of around 1×10^{-3} monolayer (ML) s^{-1}. 1 ML corresponds to 1.57×10^{15} atoms cm^{-2} for Ir(111). The amount of deposited Au was analyzed from the STM images. The base pressure during the Au deposition was kept below 6×10^{-8} Pa. The STM data were recorded in the constant current mode with tunneling currents around 0.1−0.3 nA and sample bias voltages in the range of −0.2 to +0.2 V. After Au was deposited at 100 K, the sample was cooled to 50 K at which STM measurements were performed. When the sample was annealed to 300 K, STM measurements were performed at 300 K. STM images in the present study are displayed as topographic topviews with higher areas denoted by brighter images. After the STM measurements of a sample surface, the surface was re-cleaned and a new Au layer was prepared on the clean surface.

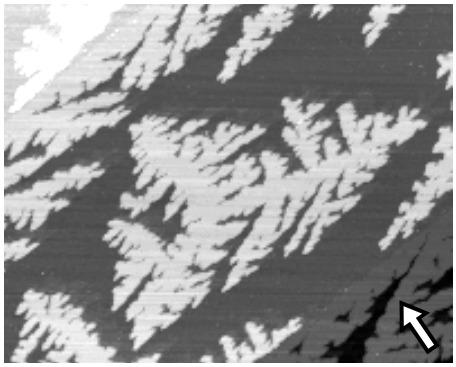

Figure 2. STM topographic image of 0.52 ML Au islands grown on Ir(111) at 300 K. The image size is 500×400 nm^2. The image was taken at a tunneling current of 0.19 nA and a sample voltage of 0.15 V. The arrow in the figure denotes the $[\bar{1}\bar{1}2]$ direction.

3. Results and discussion

3.1. Submonolayer growth at 300 K

Figure 2 shows an STM image of the 0.52 ML Au islands grown on Ir(111) at 300 K. Below one monolayer, two-dimensional dendritic islands with a monatomic height of Au are formed on the terraces and at the steps. The Au islands have a triangular envelope and their branches preferentially grow into three $\langle\bar{1}\bar{1}2\rangle$ directions rotated by 120° with respect to each other, which reflects the threefold symmetry of the Ir(111) substrate. The origin of the dendritic shape is explained by the smaller diffusion rate of Au adatoms along the Au island edge with respect to that on the Ir(111) terrace [15]. No nucleation of the second-layer islands is observed on the first-layer islands at this coverage, indicating that atoms deposited directly on an existing island can descend easily from the island, i.e. the step-down diffusion barrier is sufficiently low for adatoms to descend from the first-layer island.

3.2. Growth at 100 K and post-growth annealing effect

Figures 3(a)–(c) show STM images of the Au islands grown on Ir(111) at 100 K. Figure 3(a) shows an STM image of 0.72 ML Au deposited on Ir(111). The Au islands have a dendritic shape and their branches preferentially grow into the $\langle\bar{1}\bar{1}2\rangle$ directions. The average island size is about 15 nm. Black

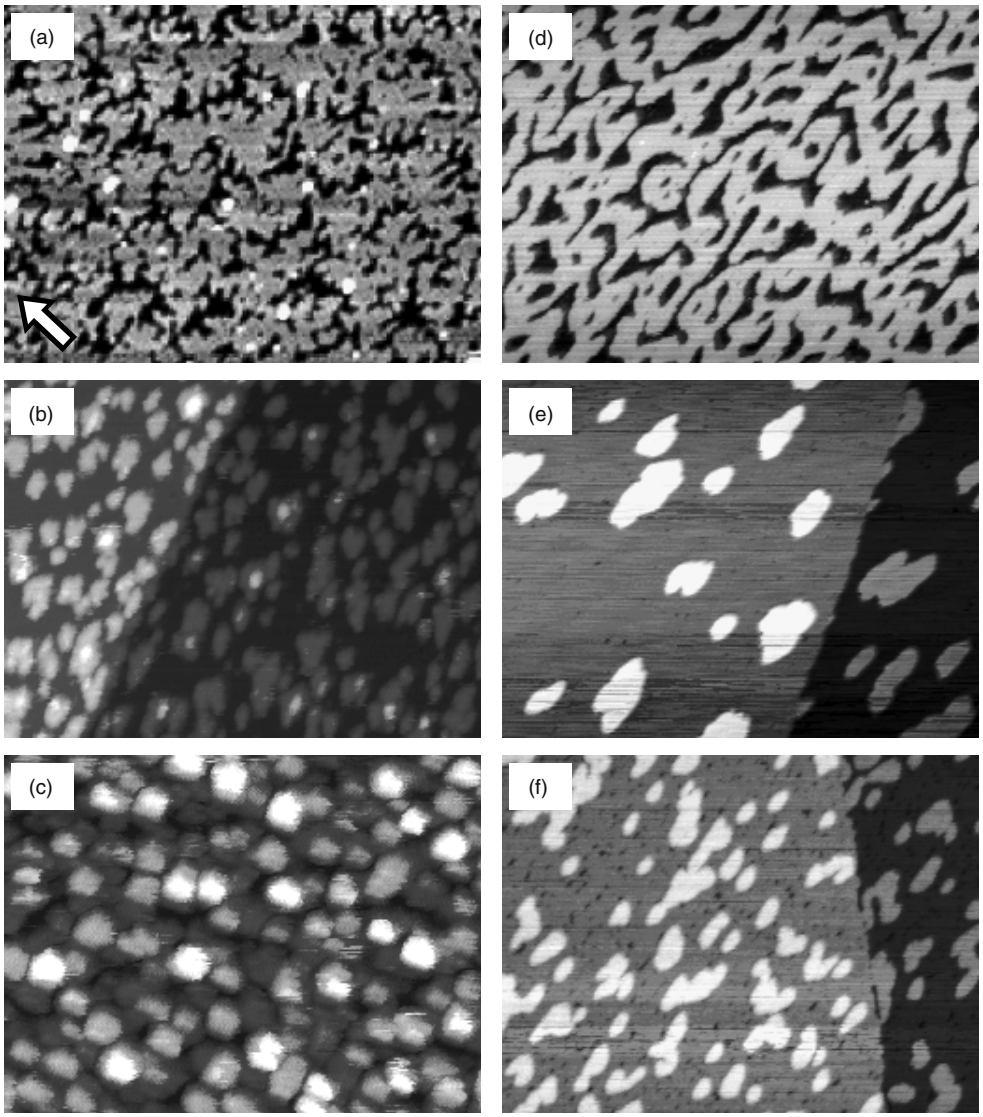

Figure 3. STM topographic images of Au islands grown on Ir(111) at 100 K (left column) and annealed to 300 K (right column). The Au coverage is (a) and (d) 0.72 ML, (b) and (e) 1.2 ML, and (c) and (f) 2.3 ML. The image size is (a) 100×75 nm^2, (b) 100×75 nm^2, (c) 50×38 nm^2, (d) 100×75 nm^2, (e) 200×150 nm^2, and (f) 200×150 nm^2. These images were taken at a tunneling current of 0.27 nA and sample voltages of (a) -0.020 V, (b) -0.080 V, (c) -0.021 V, (d) -0.050 V, (e) -0.080 V, and (f) -0.020 V. The arrow in (a) denotes the $[\bar{1}\bar{1}2]$ direction. The orientation of the sample is identical for all these images.

bars in figure 4 show experimental histograms of the exposed coverage of the Au layers at 100 K. The exposed coverage φ_L (ML) of the layer L is given by $\varphi_L = \Theta_L - \Theta_{L+1}$, where Θ_L (ML) is the coverage of the layer L and $L = 0$ is the substrate with $\Theta_0 = 1$ [16]. Even at 0.72 ML, only 1% of the area is the second-layer islands. The density of the second-layer islands is 8×10^{-5} ML. The island density in the present study is calculated by dividing the number of islands in an image by the total adsorption sites in the image calculated from the image area. Thus, the unit of the island density is ML. Obviously, the first Au layer grows in an almost complete layer at 100 K, which is consistent with the previous AES result [8]. This indicates that Au atoms deposited on top of the first-layer Au islands diffuse to the island edges and go down to the Ir substrate across the steps. In contrast to the first-layer islands, the second-layer islands at 1.2 ML have an irregularly compact shape with an average size of 5.3 nm, as shown in figure 3(b). Furthermore, the third-layer islands are formed in spite of the relatively low coverage of the second-layer islands. From the histogram of the exposed coverage shown in figure 4(b), 1.2% of the area is found to be the third-layer islands. Increasing the Au coverage up to 2.3 ML leads to the formation of higher-layer islands, as shown in figure 3(c). From the Au coverage and the height distribution of the image, the top layer in figure 3(c) is found to be the fifth layer with an average size of 2.7 nm. The average size of the fourth-layer islands is 3.7 nm. From the histogram shown in figure 4(c), the ratio of the exposed coverage between the fifth, fourth, third, second, and first Au layers is found to be 0.002:0.090:0.40:0.47:0.038. This indicates that the Au growth proceeds in a multilayer mode from the second layer.

Figures 3(d)–(f) show STM images taken after annealing the Au-covered Ir(111) surfaces shown in figures 3(a)–(c) to 300 K. At 0.72 ML, the islands coalesced with each other and

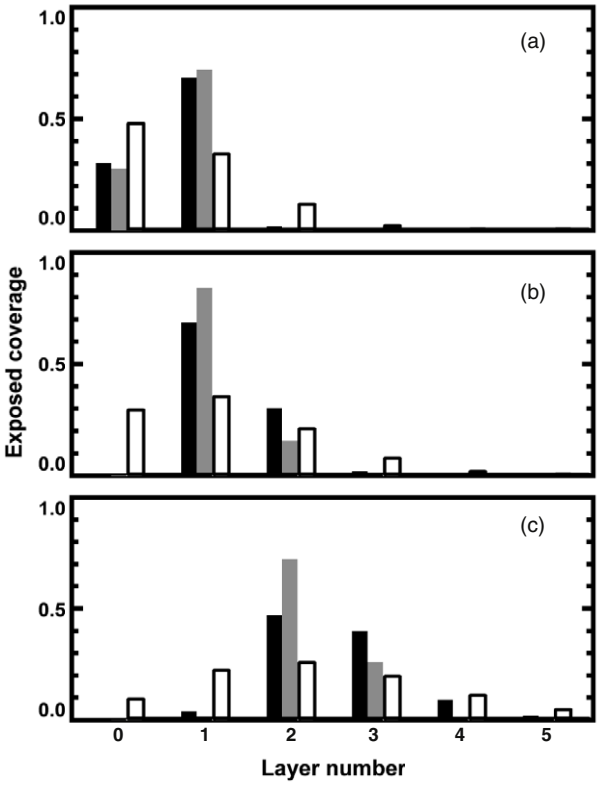

Figure 4. Experimental and theoretical histograms of exposed coverages at adsorbate coverages of (a) 0.72, (b) 1.2, and (c) 2.3 ML. Black and gray bars denote the experimental histograms taken at 100 K and after annealing to 300 K, respectively. White bars denote the calculated histograms without the interlayer diffusion, which follow the Poisson distribution. The layer number 0 means the uncovered substrate.

form an Au island network as shown in figure 3(d). Compared with the island shape at 100 K in figure 3(a), the islands in figure 3(d) have a smoother island edge. The coalescence and edge smoothing would be caused by the detachment of the atoms from the islands. The detached atoms increase the adatom flux between the islands and fill the space between the islands. The detached atoms can also attach to energetically more favored sites, i.e. higher coordinated sites after some cycles of the detachment, diffusion, and attachment [17]. Our previous study [18] revealed that the critical island size [19] is larger than 2 at 300 K, which means that the dimer dissociation occurs at 300 K. Therefore, the adatoms at the lower coordinated sites of the island would detach from the island at 300 K.

Figure 3(e) shows an STM image of the 1.2 ML Au-covered Ir(111) surface annealed to 300 K after Au deposition at 100 K. The third-layer islands formed at 100 K disappeared after the annealing. Since Au desorbs from Ir(111) above 1200 K, Au desorption is unlikely to occur. Hence, the disappearance of the third-layer islands is caused by the step-down diffusion of the atoms dissociated from the third-layer islands. If the multilayer growth were preferred thermodynamically at 100 K, the population of the third- or higher-layer islands would increase by annealing to higher temperatures. Since the STM result shows no increase of the number of the third-layer islands, the third-layer islands at 100 K are formed for a kinetics reason, i.e. by the limited step-down diffusion. The density of the second-layer islands also decreased after the annealing, as shown in figures 3(b) and (e). Since the first Au layer is almost completed at 100 K, the decrease of the number of the second-layer islands indicates that the island coalescence was caused by the adatom detachment in the same way as the first Au layer shown in figure 3(d).

Such an annealing effect is also seen in figure 3(f). Annealing the Ir(111) surface covered by 2.3 ML Au to 300 K reduced the number of the fourth- and higher-layer islands. This can be seen in the histogram of the exposed coverage, as denoted by gray bars in figure 4(c). This indicates that the detached atoms from the higher-layer islands undergo step-down diffusion, and hence the higher-layer islands decay and the first and second Au layers grow with dissipation of the higher-layer islands.

If interlayer diffusion is prohibited, the exposed coverage $\varphi_L (L \geqslant 1)$ at the total coverage of Θ follows the Poisson distribution [16]

$$\varphi_L = \frac{\exp(-\Theta)\Theta^L}{L!}. \tag{1}$$

The calculated histograms of the exposed coverage by equation (1) at total coverages of 0.72, 1.2, and 2.3 ML are shown by white bars in figure 4 together with the experimental histograms. Compared to the Poisson distribution, the experimental histograms at 100 K show lower exposed coverages of the substrate. For example, the exposed coverage of the substrate at a total coverage of 0.72 ML is about 0.5 ML without the interlayer diffusion, whereas the experimental one at 100 K is only 0.27 ML, as shown in figure 4(a). This indicates that the uncovered substrate area is filled by adatoms coming from the higher layers. Furthermore, the experimental histograms show lower exposed coverages of the top layer. For example, the exposed coverage of the third layer at a total coverage of 1.2 ML is about 0.08 ML without the interlayer diffusion, whereas the experimental one at 100 K is only 0.012 ML as shown in figure 4(b). The deviation from the Poisson distribution is caused by the interlayer diffusion. If step-down diffusion occurs, the population of the higher layers will decrease with respect to that of the Poisson distribution, whereas it will increase if step-up diffusion occurs.

Whether the interlayer diffusion takes place can be judged by the surface width W, which is the standard deviation of the film height, defined through [16]

$$W^2 = \sum_{L=0}^{\infty} (L - \Theta)^2 \varphi_L, \tag{2}$$

where Θ is the total coverage corresponding to the mean height. For statistical growth without the interlayer diffusion that results in the Poisson distribution of the exposed coverage, the surface width W_{stat} is given by $W_{\mathrm{stat}} = \sqrt{\Theta}$ [16]. $W < W_{\mathrm{stat}}$ indicates that the step-down diffusion takes place, whereas $W > W_{\mathrm{stat}}$ indicates that the step-up diffusion takes place. For ideal layer-by-layer growth, the surface width

Table 1. Experimental and theoretical surface widths at adsorbate coverages of 0.72, 1.2, and 2.3 ML. $W_{100\ \mathrm{K}}$ and $W_{300\ \mathrm{K}}$ denote the experimental surface widths measured at 100 K and after annealing to 300 K, respectively. W_{LBL} and W_{stat} denote the theoretical surface widths for layer-by-layer growth and statistical growth, respectively.

Coverage (ML)	$W_{100\ \mathrm{K}}$	$W_{300\ \mathrm{K}}$	W_{LBL}	W_{stat}
0.72	0.48	0.45	0.45	0.84
1.2	0.51	0.37	0.37	1.1
2.3	0.76	0.47	0.46	1.5

W_{LBL} is given by $W_{\mathrm{LBL}}^2 = \varphi_{L_{\mathrm{top}}}(1 - \varphi_{L_{\mathrm{top}}})$, where L_{top} is the top layer, because only the top layer is incomplete [16]. The experimentally analyzed and theoretical surface widths at respective coverages are summarized in table 1. At 0.72 ML, the experimental surface width at 100 K is 0.48, which is smaller than $W_{\mathrm{stat}} = 0.84$ and similar to $W_{\mathrm{LBL}} = 0.45$. Therefore, it can be said that the first Au layer on Ir(111) grows in an almost complete layer due to sufficient step-down diffusion. On the other hand, the surface widths at 1.2 and 2.3 ML are both $W_{\mathrm{LBL}} < W < W_{\mathrm{stat}}$ at respective coverages. This means that the second or higher Au layers grow in a multilayer fashion due to a limited step-down diffusion. The surface widths after annealing to 300 K are similar to W_{LBL} at all coverages, which indicates that the step-down diffusion is enhanced by the annealing.

3.3. Estimation of ES barriers by KMC simulations

The STM results have shown that the first Au layer on Ir(111) grows in a complete layer, whereas the second and higher Au layers grow in the multilayer mode. As described above, the step-down diffusion will be the dominant factor determining the growth mode. Thus, the layer dependence of the growth mode will be related to the layer dependence of the ES barrier. In the following, we estimate the ES barrier on each layer by performing KMC simulations with the ES barrier as a parameter. We used a KMC simulation model similar to the one used in our previous study [15]. The KMC simulation model considers the terrace, corner, and edge diffusions. The terrace diffusion is the diffusion of adatoms without in-layer neighboring atoms. The corner and edge diffusions are the diffusions from the in-layer onefold and twofold coordinated sites of the islands, respectively [20]. The terrace and edge diffusion rates are denoted by ν_{t} and ν_{edge}, respectively. The corner diffusions to the A and B steps [21] that are inherent in islands grown on an fcc(111) surface are distinguished. The A step is the {100} microfacet which is perpendicular to the $\langle\bar{1}\bar{1}2\rangle$ direction, and the B step is the {111} microfacet which is perpendicular to the $\langle 11\bar{2}\rangle$ direction. The corner diffusion rates to the A and B steps are denoted by ν_{ca} and ν_{cb}, respectively. On the other hand, the atoms at an island edge can detach from the island with a rate of ν_{detach}. The adatoms at the threefold or higher coordinated sites are assumed to be immobile and become island atoms. Atoms are deposited on an fcc(111) surface with a deposition rate of F (ML s^{-1}). The atoms in the Lth layer (on the $(L-1)$th-layer islands) diffuse randomly on the islands with a diffusion rate of $\nu_{\mathrm{t},L}$. As well as the terrace diffusion rate, the rates of all processes can be set depending on the layer. Each diffusion rate is calculated by $\nu_0 \exp(-E_{i,L}/k_{\mathrm{B}}T)$, where ν_0 is the attempt frequency, $E_{i,L}$ represents the respective diffusion barrier, k_{B} is the Boltzmann factor, and T is the temperature. ν_0 is assumed to be identical for all processes.

In the present study, the step-down and step-up diffusions are also taken into account. As shown in figure 1(a), the atoms in the $(L+1)$th layer (on the Lth-layer island) can descend from the island with a rate of $\nu_{\mathrm{down},L+1} = \nu_0 \exp[-(E_{\mathrm{t},L+1} + E_{\mathrm{down},L+1})/k_{\mathrm{B}}T]$, where $E_{\mathrm{down},L+1}$ is the ES barrier on the Lth-layer island. The atoms at the island edge can also perform the step-up diffusion onto the island. According to figure 1(a), the step-up diffusion rate $\nu_{\mathrm{up},L}$ can be given by $\nu_{\mathrm{up},L} = \nu_0 \exp[-(E_{\mathrm{up},L} + E_{\mathrm{detach},L})/k_{\mathrm{B}}T]$, where $E_{\mathrm{up},L}$ is the additional barrier for the step-up diffusion of the Lth-layer atoms as defined in figure 1(a) and $E_{\mathrm{detach},L}$ is the detachment barrier. However, we assumed that the step-up diffusion is frozen at 100 K in the present simulations, because the step-down diffusion is the dominant factor determining the growth mode as discussed above. The simulations were performed on the lattice with 400×460 adsorption sites with a periodic boundary condition. The island growth under $F = 1 \times 10^{-3}$ ML s^{-1} and $T = 100$ K was simulated.

Figures 5(a)–(c) show the simulation results at 0.72 ML. The parameters were $\nu_{\mathrm{t},1} = 5.2 \times 10^4$, $\nu_{\mathrm{ca},1} = 7.8 \times 10^1$, $\nu_{\mathrm{cb},1} = 2.4 \times 10^{-1}$, and $\nu_{\mathrm{edge},1} = 1.9 \times 10^{-16}$ s^{-1} for $L = 1$, $\nu_{\mathrm{t},L} = 2.5 \times 10^3$, $\nu_{\mathrm{ca},L} = \nu_{\mathrm{cb},L} = 2.5 \times 10^1$, and $\nu_{\mathrm{edge},L} = 2.4 \times 10^{-1}$ s^{-1} for $L \geqslant 2$, and $\nu_{\mathrm{detach},L} = 2.2 \times 10^{-6}$ s^{-1} for all layers. These parameters are based on the diffusion barriers and attempt frequencies obtained in our previous study [15, 18]. The values well reproduce the densities and shapes of the Au islands grown on Ir(111) at 100 K shown in figure 3 and those at 300 K shown in figure 2. Since ν_0 is assumed to be identical for all diffusions, the step-down diffusion rate $\nu_{\mathrm{down},L}$ is given by $\nu_{\mathrm{down},L} = \nu_{\mathrm{t},L} \exp(-E_{\mathrm{down},L}/k_{\mathrm{B}}T)$. As shown in figure 5(a), the second-layer islands hardly nucleate at 0.72 ML when the ES barrier is 0 eV. On the other hand, the number of second-layer islands increases with increasing E_{down}, as shown in figures 5(b) and (c). Since E_{down} is set to the same value for all layers, the third-layer islands also start to nucleate at larger E_{down}. To compare with the experimental data, the density of the second-layer islands (n_2) is analyzed. The simulated n_2 is shown in figure 6(a) as a function of E_{down}. By comparing the simulated n_2 with the experimental n_2 of 8×10^{-5} ML obtained from figure 3(a), E_{down} can be estimated to be 0.02 eV on the first Au layer grown on Ir(111).

Figures 5(d)–(f) show the simulation results at 1.2 ML. $E_{\mathrm{down},2}$ on the first layer was set to 0.02 eV, and island growth was simulated as a function of $E_{\mathrm{down},L}$ ($L \geqslant 3$). The other parameters were the same as those used in figures 5(a)–(c). The first layer grows in an almost complete layer, and the fraction of the uncovered substrate area is smaller than 2%. This result is consistent with the STM results, which ensures the validity of $E_{\mathrm{down},2} = 0.02$ eV. Similarly to figures 5(a)–(c), the third-layer islands start to nucleate with increasing $E_{\mathrm{down},L}$. The ratio of the third-layer island density (n_3) to n_2 is plotted as a function of $E_{\mathrm{down},L}$ in figure 6(b). By comparing the simulation

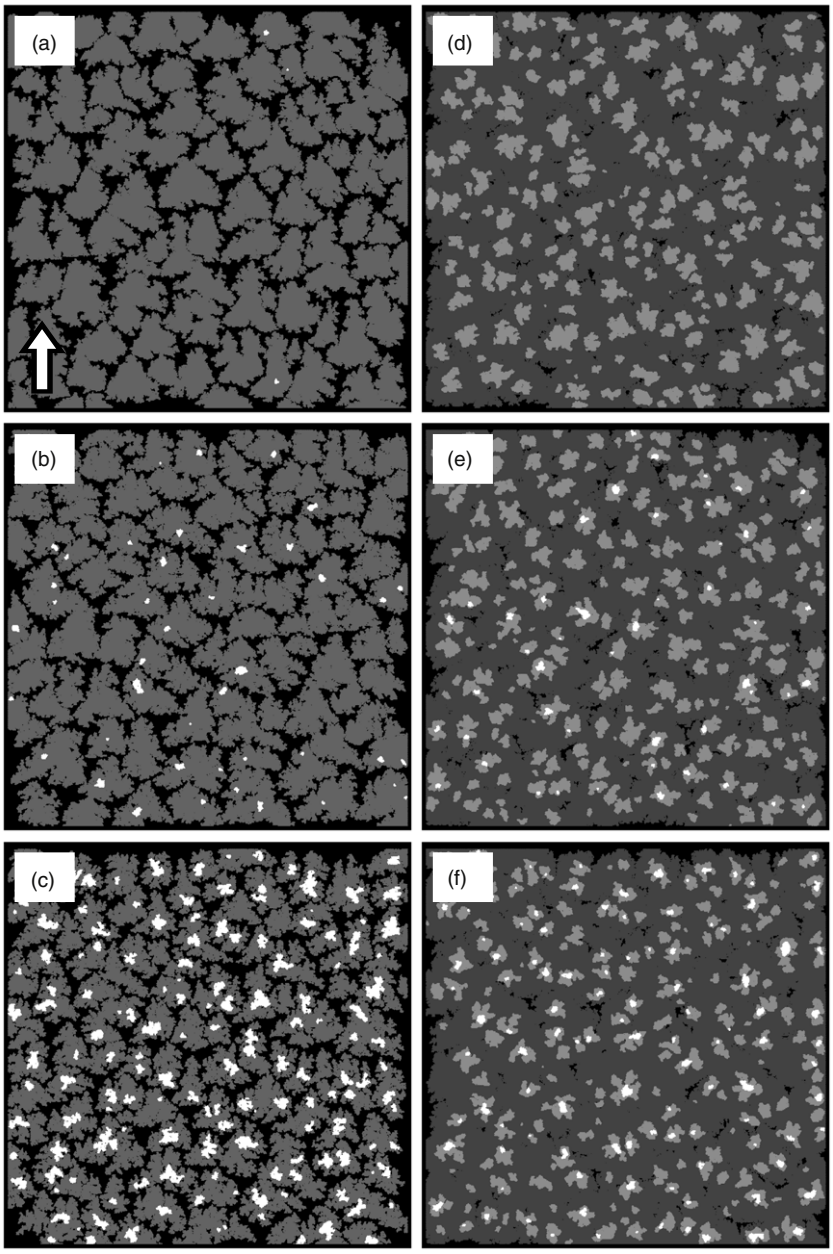

Figure 5. Simulation results at 100 K as a function of the ES barrier at (a)–(c) 0.72 ML and (d)–(f) 1.2 ML. The simulations were performed under the conditions of $F = 1 \times 10^{-3}$ ML s^{-1}, $\nu_{t,1} = 5.2 \times 10^{4}$, $\nu_{ca,1} = 7.8 \times 10^{1}$, $\nu_{cb,1} = 2.4 \times 10^{-1}$, $\nu_{edge,1} = 1.9 \times 10^{-16}$ s^{-1} for $L = 1$, $\nu_{t,L} = 2.5 \times 10^{3}$, $\nu_{ca,L} = \nu_{cb,L} = 2.5 \times 10^{1}$, $\nu_{edge,L} = 2.4 \times 10^{-1}$ s^{-1} for $L \geqslant 2$, and $\nu_{detach,L} = 2.2 \times 10^{-6}$ s^{-1} for all layers. $E_{down,L}$ is (a) 0, (b) 0.025, and (c) 0.04 eV for all layers. $E_{down,2} = 0.02$ eV in (d)–(f) and $E_{down,L}$ is (d) 0.02, (e) 0.045, and (f) 0.06 eV for $L \geqslant 3$. The lattice size corresponds to 400 × 460 adsorption sites. Brighter areas correspond to higher areas. The arrow in (a) denotes the $[\bar{1}\bar{1}2]$ direction.

results with the experimental ratio of $n_3/n_2 = 0.205$ obtained from figure 3(b), $E_{down,L}$ can be estimated to be 0.04 eV on the second Au layer grown on Ir(111).

The estimated ES barriers of $E_{down,2} = 0.02$ eV and $E_{down,L} = 0.04$ eV ($L \geqslant 3$) also reproduce the island structure at 2.3 ML as shown in figure 7. We found that $\nu_{edge,L}$ ($L \geqslant 3$) should be 2.5×10^{1} s^{-1} to reproduce the experimental island shape of the higher-layer islands. The other parameters were the same as those used in figures 5(d)–(f). The simulation result agrees well with the STM result shown in figure 3(c). The histogram of the exposed coverage also agrees with the experimental result.

The ES barrier has been estimated to be 0.02 eV on the first-layer Au islands and 0.04 eV on the second-layer Au islands. It should be noted that $\nu_{t,L}$ was assumed to be the same for $L \geqslant 2$. If $\nu_{t,3}$ on the second-layer islands is so small that the adatoms on the islands cannot arrive at the island edge, the third-layer islands nucleate even at $E_{down,3} = 0$ eV. However, since the density of the third- or higher-layer islands grown on Ir(111) at 300 K is almost the same as that of the second-layer islands [15], $\nu_{t,2}$ and $\nu_{t,3}$ are expected to be almost the same. Therefore, this assumption has little effect on the simulation results. It should also be noted that the ES barrier is assumed to be independent of the step type. A previous study reported

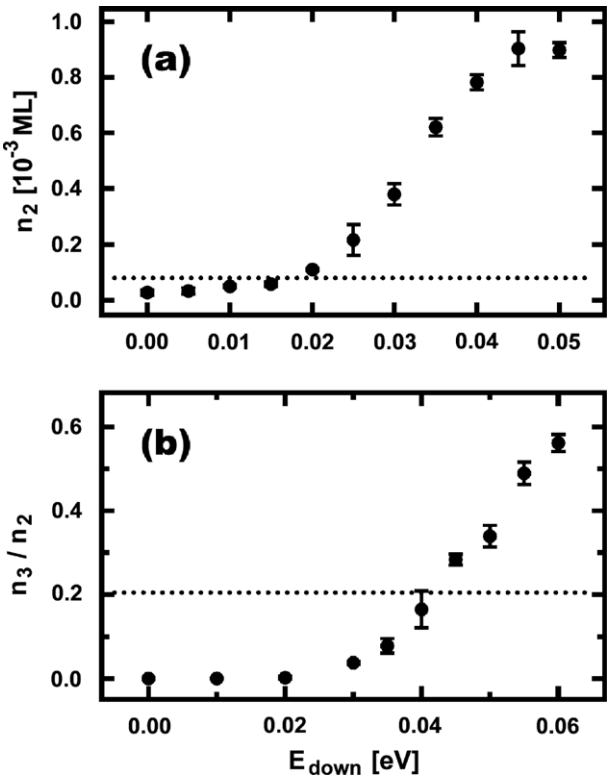

Figure 6. (a) Simulated density of the second-layer islands (n_2) at 100 K and 0.72 ML as a function of E_{down}. (b) Simulated ratio of the density of the third-layer islands (n_3) to n_2 at 100 K and 1.2 ML as a function of E_{down}. Dotted lines denote the experimental values.

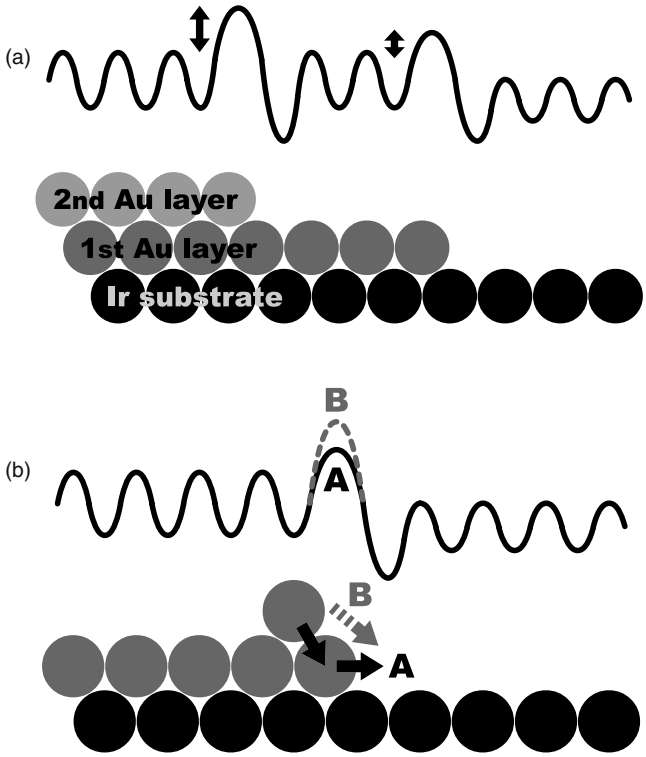

Figure 8. (a) Schematic energy diagram near the steps of the first and second Au layers grown on Ir(111). (b) Schematic energy diagram of the step-down diffusion by (A) exchange and (B) hopping mechanisms.

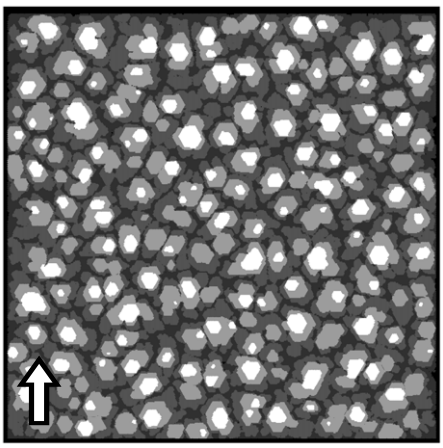

Figure 7. Simulation result at 100 K and 2.3 ML with $E_{\mathrm{down},2} = 0.02$ eV, $E_{\mathrm{down},L} = 0.04$ eV for $L \geqslant 3$, and $\nu_{\mathrm{edge},L} = 2.5 \times 10^1\ \mathrm{s}^{-1}$ for $L \geqslant 3$. The other parameters were the same as those used in figures 5(d)–(f). The arrow in the figure denotes the $[\bar{1}\bar{1}2]$ direction.

that the ES barrier is smaller at the B step than at the A step, which results in the formation of the islands mainly bounded by the B step at lower coverages and by the A step at higher coverages [7]. However, since the island orientation is found to be independent of the coverage in our STM measurements, such a step-type dependence of the ES barrier can be neglected.

In our previous study, we have estimated the ES barrier to be smaller than 0.040 eV on the first Au layer and larger than 0.040 eV on the second Au layer [22][1] by using the theory of the critical island radius for layer-by-layer growth [5] with an assumption of $\nu_{\mathrm{down}} \ll \nu_{\mathrm{t}}$. In the present study, we have estimated the ES barrier by using the KMC simulations. KMC simulations can derive the ES barrier without such an assumption. Since KMC simulations can include the island shape effect by adjusting the corner and edge diffusion rates, furthermore, the ES barriers estimated by the KMC simulations are expected to be more accurate than those obtained by the critical island radius theory where such a detailed island shape effect cannot be included. However, the estimated values by the KMC simulations agree with those obtained by the critical island radius theory. Thus, the present results show that the assumptions in the critical island radius theory have little effect on the estimation of the ES barriers in the present case.

The STM and KMC simulation results clearly show that the ES barrier on the first Au layer on Ir(111) is smaller than that on the second Au layer on Ir(111) as shown in figure 8(a). The smaller ES barrier on the first Au layer is consistently understood in terms of the lattice mismatch. Since the lattice constant of Au is larger than that of Ir by 6.3%, there is a compressive strain in the Au islands grown on Ir(111). The islands will preferentially relieve their strain at the edges where the atoms are free to expand laterally.

[1] In [22], $\alpha = \exp(-E_{\mathrm{down}}/k_{\mathrm{B}}T)$ at 100 K was estimated to be larger than 1×10^{-2} on the first Au layer and smaller than 1×10^{-2} on the second Au layer. From these results, E_{down} is estimated to be smaller and larger than 0.040 eV on the first and second Au layers, respectively.

This relaxation can facilitate the step-down diffusion by the exchange mechanism that is reported to be energetically preferred for the step-down diffusion [23–25]. A schematic illustration of the step-down diffusion by the exchange and normal hopping mechanisms and the corresponding schematic energy diagrams are shown in figure 8(b). An LEED measurement revealed that the first Au layer is compressed to match the Ir substrate, whereas the third Au layer is less compressed than the first Au layer [22]. Due to the larger compressive strain in the first Au layer, the ES barrier becomes lower on the first Au layer on Ir(111) than on the higher Au layers. It is reported that the ES barrier of Ag on the 1 ML Ag-covered Pt(111) is 0.030 eV, whereas the ES barrier of Ag on Ag(111) is 0.12 eV [6]. The smaller ES barrier on the first Ag layer on Pt(111) than on Ag(111) is attributed to the lattice mismatch effect described above. The ES barriers of 0.02 and 0.04 eV obtained in the present study are similar to that of the Ag step-down diffusion from the first Ag layer grown on Pt(111).

4. Conclusions

The growth of Au islands on Ir(111) has been investigated by STM and KMC simulations. The first Au layer on Ir(111) was found to grow in a complete layer at 100 K, whereas the Au layer grows in a three-dimensional fashion from the second Au layer at this temperature. It was also found that annealing these surfaces to 300 K reduces the higher-layer islands. By measuring the density of the top-layer islands and comparing it with the KMC simulation result, the ES barrier has been estimated to be 0.02 eV on the first Au layer and 0.04 eV on the second Au layer. The layer dependence of the ES barrier can be explained in terms of the lattice mismatch between Au and underlying layers.

Acknowledgments

This work was supported by a Grant-in-Aid for Scientific Research from the Ministry of Education, Science, Sports and Culture of Japan and CREST-JST.

References

[1] Ehrlich G and Hudda F G 1966 *J. Chem. Phys.* **44** 1039
[2] Schwoebel R L 1969 *J. Appl. Phys.* **40** 614
[3] Fu T-Y, Wu H T and Tsong T T 1998 *Phys. Rev.* B **58** 2340
[4] Fu T-Y, Tzeng Y R and Tsong T T 1996 *Phys. Rev. Lett.* **76** 2539
[5] Tersoff J, van der Gon A W D and Tromp R M 1994 *Phys. Rev. Lett.* **72** 266
[6] Bromann K, Brune H, Röder H and Kern K 1995 *Phys. Rev. Lett.* **75** 677
[7] Li M, Chung P W, Cox E, Jenks C J, Thiel P A and Evans J W 2008 *Phys. Rev.* B **77** 033402
[8] Okada M, Nakamura M, Moritani K and Kasai T 2003 *Surf. Sci.* **523** 218
[9] Okada M, Moritani K, Kasai T, Diño W A, Kasai H, Ogura S, Wilde M and Fukutani K 2005 *Phys. Rev.* B **71** 033408
[10] Okada M, Ogura S, Diño W A, Wilde M, Fukutani K and Kasai T 2005 *Appl. Surf. Sci.* **246** 68
[11] Okada M, Ogura S, Diño W A, Wilde M, Fukutani K and Kasai T 2005 *Appl. Catal.* A **291** 55
[12] Haruta M 1997 *Catal. Today* **36** 153
[13] Ruff M, Frey S, Gleich B and Behm R J 1998 *Appl. Phys.* A **66** S513
[14] Barredo D, Calleja F, Nieto P, Hinarejos J J, Laurent G, de Parga A L V, Farías D and Miranda R 2008 *Adv. Mater.* **20** 3492
[15] Ogura S, Fukutani K, Matsumoto M, Okano T, Okada M and Kawamura T 2006 *Phys. Rev.* B **73** 125442
[16] Michely T and Krug J 2004 *Islands, Mounds, and Atoms* (Berlin: Springer)
[17] Xu Y-Q, Liu B-G, Wang E G and Wang D-S 2001 *J. Phys. D: Appl. Phys.* D **34** 1137
[18] Ogura S and Fukutani K 2008 *J. Phys.: Conf. Ser.* **100** 072003
[19] Venables J A 1973 *Phil. Mag.* **27** 697
[20] Brune H, Röder H, Bromann K, Kern K, Jacobsen J, Stoltze P, Jacobsen K and Nørskov J 1996 *Surf. Sci.* **349** L115
[21] Wang S C and Ehrlich G 1991 *Phys. Rev. Lett.* **67** 2509
[22] Ogura S, Fukutani K and Okada M 2007 *Top. Catal.* **44** 65
[23] Jacobsen J, Jacobsen K W, Stoltze P and Nørskov J K 1995 *Phys. Rev. Lett.* **74** 2295
[24] Stumpf R and Scheffler M 1994 *Phys. Rev. Lett.* **72** 254
[25] Li Y and DePristo A E 1994 *Surf. Sci.* **319** 141